Analysis of Non-innocence of Phosphaquinodimethane Ligands when Charge and Aromaticity Come into Play

Philip Junker,[a] Alicia Rey Planells,[b] Arturo Espinosa Ferao,*[b] and Rainer Streubel*[a]

Dedicated to Prof. Dr. Masaaki Yoshifuji on the occasion of his 80th birthday.

Abstract: Several phosphaquinodimethanes and their $M(CO)_5$ complexes (M = Cr, Mo, W) and model derivatives have been theoretically investigated regarding the quest of non-innocence. Computed structural and electronic properties of the *P*-Me/NH_2 substituted phosphaquinodimethanes and tungsten complexes revealed an interesting non-innocent ligand behaviour for the radical anion complexes with distonic ion character and a strong rearomatization of the middle phenyl ring. The latter was further probed taking also geometric aromaticity (HOMA) and quinoid distortion parameters (HOMQc) into account, as well as NICS(1). Furthermore, the effect of the P-substitution was investigated for real (or plausible) complexes and their free ligands focusing on the resulting aromaticity at the middle phenyl ring and vertical one-electron redox processes. The best picture of ligand engagement in redox changes was provided by representing NICS(1) values versus HOMA and the new geometric distortion parameter HOMQc8.

Introduction

In general, paramagnetic compounds play an important role in synthetic and analytical chemistry.[1] Nevertheless, compounds bearing localized unpaired electrons at a main group element are very reactive and remain rare. Known examples share structural motives, *e.g.*, sterical bulk or π-delocalization to gain stability.[2] In this connection the element Phosphorus was often investigated as a bound element due to its ability to localize and delocalize unpaired electrons.[3] Further stabilization of such compounds can also be achieved through transition metal complexation. Reactive paramagnetic transition metal complexes and their intermediates have been studied extensively for their important role in catalytic processes for a long time.[4] Much of the chemistry of paramagnetic transition metal complexes depends on the localization of the unpaired electron, *i.e.*, the spin density distribution, especially if most is localized on either the metal centre or the ligand. For most paramagnetic complexes, the unpaired electron is localized at the metal centre,[5] whereas those bearing most of the unpaired electron at the ligand remain rare and, therefore, very interesting. These so-called non-innocent ligands participate strongly in the open-shell chemistry of the corresponding paramagnetic complexes.[6] Until today there are only a few complexes known bearing such kind of non-innocent P-ligands.[7–11] Therefore, the knowledge on the properties and capabilities of open-shell P-ligands in coordination chemistry is still scarce and, hence, research is ongoing.

So far, classical concepts relied on the coordination of stable or transient P-ligands such as phosphinyl (IUPAC: phosphanyl).[7] More recently, the radical formation was achieved within the ligand entity thus resulting in highly reactive group 6 metal complexes such as P-functional phosphinyl complexes **I**[8] or phosphanoxyl complexes **II**.[9] Other, readily accessible redox-active ligands (in complexes) are phosphaalkenes **III**[10] and *p*-phosphaquinodimethanes **IV** (Scheme 1).[11]

Electronic structures of group 6 metal complexes (**III**, **IV**) were investigated theoretically for the first time, focusing on

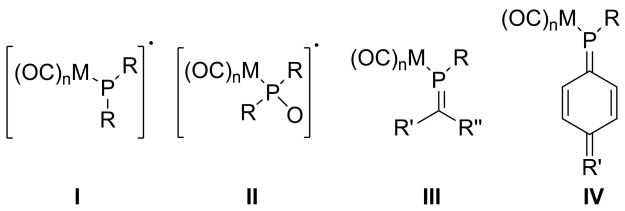

I **II** **III** **IV**

Scheme 1. Examples of known short-lived open-shell complexes (**I**, **II**) and those with redox active P-ligands (**III**, **IV**) (M: transition metal, R: organic substituent).

[a] *Dr. P. Junker, Prof. Dr. R. Streubel*
Institut für Anorganische Chemie
Rheinische Friedrich-Wilhelms-Universität Bonn
Gerhardt-Domagk-Straße 1, 53121 Bonn (Germany)
E-mail: r.streubel@uni-bonn.de
Homepage: https://www.chemie.uni-bonn.de/akstreubel/prof.-dr.-streubel

[b] *A. Rey Planells, Prof. Dr. A. Espinosa Ferao*
Departamento de Química Orgánica, Facultad de Química
Universidad de Murcia
Campus de Espinardo, 30100 Murcia (Spain)
E-mail: artuesp@um.es
Homepage: http://www.um.es/funcmolecmat/artuesp

Supporting information for this article is available on the WWW under https://doi.org/10.1002/chem.202100420

bond dissociation energies (BDEs), frontier molecular orbitals (FMOs) and charge distributions.[12] One important result was that radical cations are most often metal-centred, whereas radical anions are ligand-centred. Among these systems, the phosphaquino-dimethane ligand remained the least investigated – theoretically and experimentally – despite being the most promising non-innocent ligand.[12] Such complexes also inherently have the possibility to form distonic radical ions, *i.e.*, having a separation of charge and radical sites.[13] Recently, we unveiled the radical formation pathway of *P*-CPh_3 substituted phosphaquinodimethane complexes and demonstrated a reversible one-electron reduction via cyclovoltammetry.[14]

Herein, theoretical studies on a broad range of *p*-phosphaquinodimethane (pPQDM) "free" ligands as well as the corresponding group 6 pentacarbonyl complexes (Cr, W) are presented, focusing on the dependence of redox properties (non-innocent behaviour) for differently charged redox states on the nature of the P-substituent (R = CPh_3, NPh_2, $CH(SiMe_3)_2$).

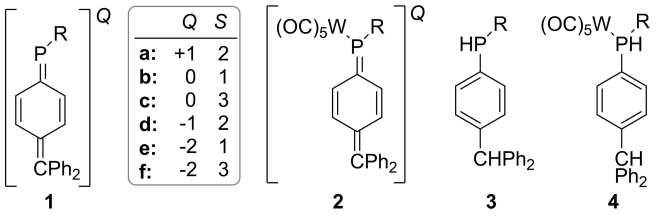

Scheme 2. Computed pPQDM model systems as free ligand **1**, their metal complexes **2** and fully aromatic references **3** and **4**.

Results and Discussion

Two pPQDMs bearing model Me and NH_2 substituents at P were computed as free ligands (**1**) and as *P*-$W(CO)_5$ complexes (**2**) (Scheme 2). For each of them, six different situations were computed with charges (Q) varying from +1 to −2 and considering the two possible spin states – singlet and triplet ($S = 1, 3$) – for neutral and dianionic species to get insight into possible diradical properties favoured by rearomatization of the ring. Fully aromatic derivatives (**3** and **4**) were also computed as references, only in their neutral (singlet) state (Scheme 2). The structures were optimized and computed using B3LYP-D3 as functional (see the Computational Details section).

Electronic distribution and exocyclic bond strengths

Herein, the focus was on bond lengths for key bonds, the Löwdin charges at relevant parts of the molecules and HOMO-LUMO gaps (chemical hardness, η) (Table 1). Structural parameters and Kohn-Sham orbitals for all molecules studied are given in the Supporting Information.

Neutral (**b**,**c**) and dianionic derivatives (**e**,**f**) were computed in their open-shell singlet and triplet electronic states (see the Supporting Information for singlet-triplet gaps) since the latter has strong influence on their structural and electronic properties (Table 1). As expected, most stable neutral singlet species (**b**) ($\Delta E_{S/T} = 9.30$–9.99 kcal/mol) display close-shell nature with the shortest exocyclic C_{exo}–C_{ring}/P–C_{ring} bonds and highest double bond character according to the Mayer Bond Order

Table 1. Computed (B3LYP-D3/def2-TZVP(ecp)/COSMO(THF)) structural (Å) and electronic parameters of the model compounds **1**–**4**.[a]

Q/S		d(C–Cring)	d(P–C_{ring})	MBO(C–C_{ring})	MBO(P–C_{ring})	MBO(P–W)	MBO(P–R)	E_{HOMO}/eV	E_{LUMO}/eV	η/eV
+1/2	**1a-Me**	1.429	1.774	1.125	1.290	–	1.057	–	−4.32	2.11
	1a-NH_2	1.424	1.752	1.157	1.299	–	1.346	−5.88	−3.90	1.98
	2a-Me	1.423	1.751	1.152	1.224	1.021	0.987	−5.93	−4.19	1.74
	2a-NH_2	1.424	1.744	1.157	1.191	0.998	1.270	−5.75	−3.83	1.92
0/1	**1b-Me**	1.383	1.719	1.393	1.655	–	1.052	−5.03	−2.66	2.37
	1b-NH_2	1.383	1.709	1.412	1.607	–	1.160	−4.62	−2.24	2.38
	2b-Me	1.385	1.708	1.381	1.473	0.795	0.958	−4.98	−2.84	2.14
	2b-NH_2	1.382	1.696	1.414	1.434	0.813	1.124	−4.75	−2.49	2.26
0/3	**1c-Me**	1.471	1.809	0.974	1.175	–	1.064	−4.43	−0.80	3.63
	1c-NH_2	1.468	1.809	0.987	1.169	–	1.181	−4.18	−0.77	3.41
	2c-Me	1.465	1.796	0.994	1.059	0.895	0.972	−6.18	−3.46	2.72
	2c-NH_2	1.462	1.803	1.008	0.924	0.771	1.167	−4.51	−1.63	2.88
−1/2	**1d-Me**	1.427	1.773	1.186	1.455	–	1.081	−3.37	−1.41	1.96
	1d-NH_2	1.427	1.766	1.196	1.443	–	1.014	−3.18	−1.24	1.94
	2d-Me	1.445	1.814	1.083	1.044	0.670	0.976	−4.19	−1.99	2.20
	2d-NH_2	1.445	1.812	1.087	1.009	0.646	1.030	−4.21	−1.98	2.23
−2/1	**1e-Me**	1.488	1.813	0.889	1.365	–	1.110	−1.92	1.01	2.93
	1e-NH_2	1.488	1.818	0.893	1.324	–	0.957	−1.89	1.03	2.92
	2e-Me	1.472	1.830	0.981	0.960	0.671	0.971	−2.20	−0.11	2.09
	2e-NH_2	1.469	1.823	0.998	0.963	0.676	1.015	−2.18	−0.12	2.06
−2/3	**1f-Me**	1.442	1.788	1.121	1.444	–	1.095	−0.15	1.05	1.20
	1f-NH_2	1.442	1.790	1.124	1.399	–	0.977	−0.14	1.09	1.23
	2f-Me	1.442	1.781	1.120	1.235	0.358	0.983	−1.01	0.26	1.27
	2f-NH_2	1.441	1.778	1.120	1.179	0.331	1.009	−1.10	0.32	1.42
0/1	**3-Me**	1.521	1.834	0.872	0.942	–	1.011	−6.26	−0.77	5.49
	3-NH_2	1.521	1.832	0.871	1.033	–	1.130	−6.02	−0.71	5.31
	4-Me	1.520	1.814	0.882	0.951	0.711	0.989	−5.99	−1.61	4.38
	4-NH_2	1.521	1.810	0.884	0.946	0.747	1.113	−6.01	−1.62	4.39

[a] Mayer bond orders (MBO), HOMO and LUMO energies and their difference (η).

(MBO)[15] values (range 1.381–1.414 and 1.434–1.655 for the C_{exo}–C_{ring} and P–C_{ring} bonds, respectively). By contrast, within pPQDMs the larger deviation towards single exocyclic bonds (MBO range 0.974–1.008 for the C_{exo}–C_{ring} and 0.924–1.175 for P–C_{ring} bonds) corresponds to neutral triplet species **c** displaying significant bi-radical character. Singlet dianions (**e**) are also more stable than their triplet counterparts (**f**) ($\Delta E_{S/T} = 27.53$–32.21 kcal/mol) and has in total the longest C_{exo}–C_{ring}/P–C_{ring} bonds (also lowest MBO for all C_{exo}–C_{ring} bonds, holding almost true for P–C_{ring} bonds), indicating partial significant occupation of the π^*(C–C) and π^*(P–C) orbitals and therefore less double bond character which also result in higher aromaticity for the central ring (*vide infra*). Absolute references for fully aromatic derivatives are found for *p*-diphenylmethyl-phosphabenzene derivatives **3** and **4** (MBO range 0.871–0.884 and 0.942–1.033 for the C_{exo}–C_{ring} and P–C_{ring} bonds, respectively).

Electric charges arising from the Löwdin population analysis[16] were employed due to their small basis set dependence.[17] The MBO values for the P–W bonds strongly correlate with the charge of the system, decreasing with the increase of negative charge. This is of course the result of stabilization effects with partial occupation of the σ^*(P–W) orbital thus leading to significant P–W bond elongations (*e.g.* $d_{P-W} = 3.01$ Å for **2f-NH$_2$**). The same behaviour can be seen for NH_2-substitution starting from MBO for the P–N bond of 1.346 (**1a-NH$_2$**) and 1.270 (**2a-NH$_2$**), due to the +M-effect of the N towards the positively charged system, and decreasing in the dianionic counterparts to 0.957/0.977 (**1e/f-NH$_2$**) and 1.015/1.009 (**2e/f-NH$_2$**), respectively.

The chemical hardness (approximated as the HOMO-LUMO gap) changes significantly depending on the electric charge and spin state of the system. The complexes (**2**) show smaller gaps than the corresponding free systems for the cationic (**a**), neutral (**b**,**c**), and closed-shell dianionic (**e**) systems, whereas the opposite is observed for the open-shell mono- and dianionic systems (**d**–**f**). As expected, the greatest chemical hardness is observed for the fully aromatic reference compounds **3** and **4**.

When looking at the (Löwdin) electric charge at phosphorus, q^L(P), the electron withdrawing character of the $W(CO)_5$ group results in the major part of the negative charge being located at the metal centre (Table 2). The outcome is a significantly higher q^L(P) for all complexes (**2**,**4**) by 0.12–0.48 a.u. compared to the corresponding free ligands (**1**,**3**), the lowest and highest differences corresponding to cationic (**a**) and dianionic (**e**,**f**) species, respectively.

In the radical-cation species, for **1a-Me** the spin density is mainly located at P (0.572 a.u.) and either the replacement of *P*-Me by *P*-NH_2 (**1a-NH$_2$** 0.235 a.u.) or addition of the metal fragment (**2a-Me** 0.243 a.u.), or both (**2a-NH$_2$** 0.127 a.u.), pushes the unpaired electron to the trityl-derived ($Ph_2CC_6H_4$) fragment. In general, the spin density at the $PW(CO)_5$ moiety increases on going from the cationic (**a**) to the triplet dianionic systems (**f**), although almost vanishes for the radical anions (**2d**) in agreement with the proposed major Lewis structure which represents a trityl group-centred unpaired electron with the negative charge located at the $PW(CO)_5$ moiety (Scheme 3), as observed (Table 2). The strong spin density delocalization should also result in a small structural change of the ligand upon one-electron-reduction, which should strongly contribute to the

Table 2. Computed (B3LYP-D3/def2-TZVP(ecp)/COSMO(THF)) electronic parameters ($q^{L\,[a]}$ $spin^{L[b]}$) for model compounds (R = Me o NH_2) **1**–**4**.

Q/S		q^L(P)	$spin^L$(P)	$q^L(C_{benzyl})$	$spin^L(C_{benzyl})$	$q^L(PW(CO)_5)$	$spin^L(PW(CO)_5)$	q^L(PR)	$spin^L$(PR)
+1/2	**1a-Me**	0.609	0.572	0.067	0.093	–	–	0.503	0.624
	1a-NH$_2$	0.615	0.235	0.037	0.214	–	–	0.773	0.341
	2a-Me	0.775	0.243	0.049	0.154	0.609	0.469	0.758	0.267
	2a-NH$_2$	0.738	0.127	0.029	0.248	0.569	0.203	0.941	0.181
0/1	**1b-Me**	0.436	–	−0.016	–	–	–	0.276	–
	1b-NH$_2$	0.446	–	−0.043	–	–	–	0.481	–
	2b-Me	0.697	–	−0.013	–	0.234	–	0.634	–
	2b-NH$_2$	0.659	-	−0.036	–	0.240	–	0.759	–
0/3	**1c-Me**	0.461	0.753	−0.006	0.399	–	–	0.304	0.820
	1c-NH$_2$	0.348	0.664	−0.007	0.396	–	–	0.353	0.838
	2c-Me	0.688	0.572	−0.006	0.393	0.270	0.808	0.614	0.630
	2c-NH$_2$	0.594	0.561	−0.006	0.388	0.125	0.733	0.681	0.721
−1/2	**1d-Me**	0.165	0.359	−0.082	0.203	–	–	−0.069	0.391
	1d-NH$_2$	0.167	0.441	−0.100	0.153	–	–	0.050	0.506
	2d-Me	0.398	0.052	−0.026	0.344	−0.349	0.081	0.218	0.057
	2d-NH$_2$	0.350	0.051	−0.026	0.343	−0.435	0.082	0.269	0.053
−2/1	**1e-Me**	−0.094	–	−0.148	–	–	–	−0.389	–
	1e-NH$_2$	0.164	–	−0.148	–	–	–	−0.354	–
	2e-Me	0.380	–	−0.145	–	−0.469	–	0.185	–
	2e-NH$_2$	0.343	–	−0.144	–	−0.561	–	0.246	–
−2/3	**1f-Me**	0.029	0.187	−0.077	0.296	–	–	−0.237	0.205
	1f-NH$_2$	−0.038	0.188	−0.078	0.294	–	–	−0.205	0.197
	2f-Me	0.346	0.228	−0.050	0.291	−1.040	1.015	0.135	0.247
	2f-NH$_2$	0.284	0.236	−0.052	0.285	−1.098	1.020	0.166	0.256
0/1	**3-Me**	0.414	–	−0.121	–	–	–	0.272	–
	3-NH$_2$	0.348	–	−0.121	–	–	–	0.315	–
	4-Me	0.682	–	−0.120	–	0.187	–	0.632	–
	4-NH$_2$	0.597	–	−0.120	–	0.108	–	0.652	–

[a] Löwdin electric charge (au); [b] Löwdin spin population (au).

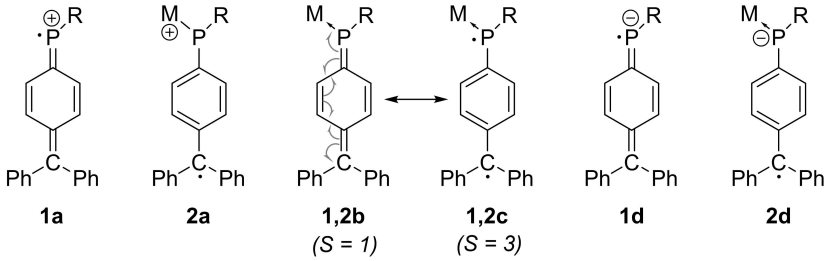

Scheme 3. Lewis structures for the pPQDM moiety on changing the electronic state of neutral compounds **1**–**2** from singlet (**b**) to triplet (**c**) and most likely description of the one-electron oxidation (**a**) and reduction (**d**) products (R = Me, NH_2; M = LP, $W(CO)_5$).

reversibility of this redox process as reported beforehand.[11] It also gives strong evidence for the non-innocence of such pPQDM ligands in group 6 metal complexes regarding one-electron reduction. All **2 d** complexes also show significantly higher Löwdin spin population at the central C atom of the formal trityl moiety (C_{benzyl}) than in both the un-ligated **1 d** and the cationic **2 a** systems (Table 2). Singlet dianions (**e**) display a complete charge separation between the $PW(CO)_5$ moiety (q^L = −0.469 and 0.561 a.u. for **2 e-Me** and **2 e-NH_2**, respectively) and the trityl-derived fragment.

Aromaticity of the central ring

Aromaticity is a multidimensional concept that can be approached and quantified from the energetic, magnetic and geometric perspectives, and even electron density descriptors (such as para-delocalization, PDI,[18] aromatic fluctuation, FLU,[19] and others) have been used with this aim. In order to check the inherent aromaticity of the middle C_6H_4 ring in the proposed major resonance structures of **2 a**, **1**,**2 c** and **2 d** compared to quinoid structures for **1 a**, **1**,**2 b** and **1 d** (Scheme 3), NICS(1)[20] (nucleus independent chemical shift at 1 Å above and below the ring centroid) values were computed at the GIAO B3LYP-TZVPPD level of theory (Table 3) (see the Computational Details). Benzene (NICS(1) = −9.90 ppm) and **3-Me**/**3-NH_2**/**4-Me**/**4-NH_2** (NICS(1) = −9.38/−8.92/−9.16/−9.10 ppm, respectively), computed at the same level, can be used as reference. According to the NMR chemical shift convention the data is displayed with negative NICS shifts denoting aromaticity, while positive describe antiaromaticity. As geometric aromaticity-related parameter, the Harmonic Oscillator Model of Aromaticity (HOMA)[21] values were also computed at the optimization level (B3LYP-D3/def2-TZVP/COSMO(THF)), referenced against benzene (HOMA = 1.000) at the same level (**3-Me/3-NH_2/4-Me/4-NH_2** HOMA = 0.996–1.000). According to both parameters, the most aromatic compounds are the neutral diradicals **c** (0/3) which require strong spin separation generating a 1,6-diradical with a rearomatized middle ring. Also singlet dianions (**e**) exhibit the expected high aromatic character and remarkable aromaticity is observed for the corresponding triplet states (**f**) as well. Noteworthy is that not only complexed radical cations (**2 a**) but also the corresponding unligated species (**1 a**) display significant aromatic character. As expected, the least aromatic compounds turn out to be the singlet neutral compounds **b**, owing to their quinoid character. The biggest difference between unligated and complexed species is again displayed by radical anions whose rather nonaromatic unligated species (**1 d**) become significantly aromatic on complexation (**2 d**). Similar (although lower) increase in aromaticity is observed from unligated singlet dianions (**1 d**) to their complexes (**2 d**).

Structural distortion of the *p*-quinodimethane moiety

In order to allow a more specific quantification of the distortion from fully aromatic to quinoid structures using rather easily accessible geometric data, a new geometric distortion parameter has been defined and named as HOMQc (*Harmonic Oscillator Model of Quinodimethane character*), by analogy to HOMA and related HOMFc (fulvenoid character)[22] and HOMCEc (conjugated ethylene character)[23] descriptors. Two different versions of the parameter were computed for the case of using only the endocyclic bond lengths (6 bonds, named as HOMQc6) or the

Table 3. Computed (GIAO B3LYP/def2-TZVPPD//B3LYP-D3/def2-TZVP/COSMO(THF)) NICS(1) (ppm) and HOMA (in parenthesis) values for model compounds **1** and **2** in all studied charge/multiplicity (Q/S) electronic configurations.

	+1/2 (**a**)	0/1 (**b**)	0/3 (**c**)	−1/2 (**d**)	−2/1 (**e**)	−2/3 (**f**)
1-Me	−6.42	−2.20	−7.60	−3.63	−4.81	−4.09
	(0.845)	(0.415)	(0.965)	(0.780)	(0.940)	(0.835)
1-NH_2	−5.66	−1.63	−7.36	−3.34	−4.64	−4.11
	(0.809)	(0.403)	(0.968)	(0.774)	(0.954)	(0.847)
2-Me	−5.87	−2.48	−7.43	−5.93	−6.38	−3.02
	(0.817)	(0.465)	(0.967)	(0.922)	(0.963)	(0.846)
2-NH_2	−5.53	−1.73	−7.40	−5.92	−6.11	−3.45
	(0.823)	(0.409)	(0.969)	(0.926)	(0.957)	(0.847)

extended structure including the two exocyclic bonds as well (8 bonds, named as HOMQc8) (Figure 1). For the HOMQc8 parameter, the exocyclic C–P bond distances were previously converted into the corresponding virtual C–C bonds having the same Pauling Bond Order (PBO), so that compounds **1** or **2** could be treated as all-carbon (virtual) *p*-quinodimethane species. Transformation of C–P into virtual C–C bonds requires the calculation of a small set of simple model molecules having pure single C(sp^2)-E or pure double C(sp^2)=E bonds (E=C, P) as references (see the Supporting Information).

By analogy with HOMA and related parameters, HOMQc6 (eq. 3) was divided into two addends, one accounting for the deviation of bond lengths (R_i) relative to the average (R_{av}) (geometric distortion, GEO_6, eq. 1) and the other reflecting the deviation of the latter from an optimal bond distance (R_{opt}) (enlargement distortion, EN, eq. 2). In case of HOMQc6, the dominant GEO component is a normalized summation over the total set of bonds with every addend being multiplied by a $(-1)^i$ factor that makes positive contributions for even bonds shorter and odd bonds larger than the average, according to the numbering scheme sketched in Figure 1 (only bonds 2–4 and 6–8 are considered). The opposite situations give rise to negative contributions. This tends to produce vanishing values for aromatic derivatives but relatively large positive values (after multiplication by the positive normalization α factor) for quinoid structures with pronounced alternating bond length patterns in odd and even bonds. The EN component makes use of a R_{opt} normalization constant.

$$GEO_6 = \frac{\alpha}{6}\sum_{i=1}^{6}(R_{av} - R_i)|R_{av} - R_i|(-1)^i \quad (1)$$

$$EN = \alpha\left(R_{av} - R_{opt}\right)\left|R_{av} - R_{opt}\right| \quad (2)$$

$$HOMQc6 = GEO_6 + EN \quad (3)$$

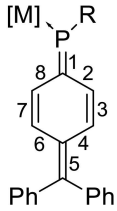

Figure 1. Numbering of bonds for HOMQc6/8 calculation in compounds **1**, **2**.

In case of HOMQc8, a positive GEO_8 component requires inverse contributions of odd and even bonds and hence a $(-1)^{i-1}$ factor was used (eq. 4). However, the GEO_8 summation is larger for aromatic compounds, therefore requiring an opposite contribution to the final geometric distortion HOMQc8 parameter (eq. 5). The required normalization constants to achieve values from 0.000 (fully aromatic *p*-xylene) to 1.000 (fully quinoid all-carbon *p*-quinodimethane) for HOMQc6/HOMQc8 are $\alpha = 298.471/133.593$ and $R_{opt} = 1.3963/1.3466$ Å, respectively. Both distortion parameters are collected in Table 4.

$$GEO_8 = \frac{\alpha}{8}\sum_{i=1}^{8}(R_{av} - R_i)|R_{av} - R_i|(-1)^{i-1} \quad (4)$$

$$HOMQc8 = 1 - (GEO_8 + EN) \quad (5)$$

Due to their definition, HOMQc6 and HOMQc8 values should vary in the range of 0–1 although higher or lower values can be observed mainly due to an imperfect C–P to virtual C–C bond length conversion. Indeed, fully aromatic reference compounds **3-Me/3-NH$_2$/4-Me/4-NH$_2$** display distortion values as low as HOMQc6 0.002/0.001/−0.001/−0.001 and HOMQc8 −0.361/−0.347/−0.240/−0.224, respectively. As the definition of HOMQc6 is similar to HOMA, although with different (reversed) normalization limits and using signed (unlike HOMA) summation of quadratic differences, the almost perfect linear correlation between these two parameters was predictable (Figure 2). It can be clearly seen that also according to geometric distortion HOMQc8, compounds **b** (0/1) display by far the lowest aromaticity (HOMQc > 0.51) in line with their expected mostly quinoid Lewis structure (Scheme 3) and scarcely aromatic NICS(1) and HOMA values (Table 3). Next are compounds **a** (+1/2), **1 d** (−1/2) and **f** (−2/3) with HOMQc8 in the 0.1–0.4 range. Low quinoid character (HOMQc < 0.06), and hence high expected aromaticity, is displayed in case of **c** (0/3), **e** (−2/1) and **2 d** (−1/2) arising from a strong 1,6-charge/spin distribution resulting in rearomatization of the middle ring. Again, as mentioned above, a big difference is observed between the moderately high quinoid character of **1 d** (−1/2) and the low values exhibited by their complexes **2 d** (Table 4).

Aromaticity indices such as HOMA (Figure 3) and NICS(1) (Figure 4) also exhibit a remarkable (second-order polynomial or linear) correlation with the geometric distortion parameter HOMQc8. Representation of HOMA (Figure 3) only shows a well-separated different area for highly quinoid scarcely aromatic neutral singlet (**b**) derivatives. However, three different regions

Table 4. Computed (B3LYP-D3/def2-TZVP/COSMO(THF)) HOMQc6 and HOMQc8 (in parenthesis) values for model compounds **1** and **2**.

	+1/2 (**a**)	0/1 (**b**)	0/3 (**c**)	−1/2 (**d**)	−2/1 (**e**)	−2/3 (**f**)
1 a-Me	0.159	0.627	0.029	0.224	0.048	0.160
	(0.240)	(0.516)	(−0.028)	(0.192)	(−0.160)	(0.102)
1 a-NH$_2$	0.199	0.637	0.029	0.227	0.037	0.149
	(0.332)	(0.545)	(−0.020)	(0.221)	(−0.175)	(0.100)
2 a-Me	0.190	0.574	0.031	0.074	0.031	0.155
	(0.342)	(0.549)	(0.063)	(0.029)	(−0.149)	(0.159)
2 a-NH$_2$	0.184	0.628	0.029	0.072	0.037	0.153
	(0.363)	(0.588)	(0.041)	(0.043)	(−0.103)	(0.177)

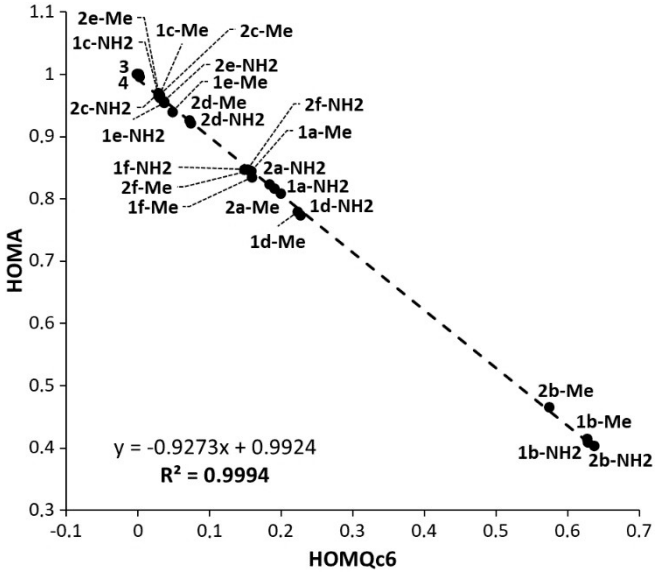

Figure 2. HOMA values plotted against HOMQc6 with a linear fit.

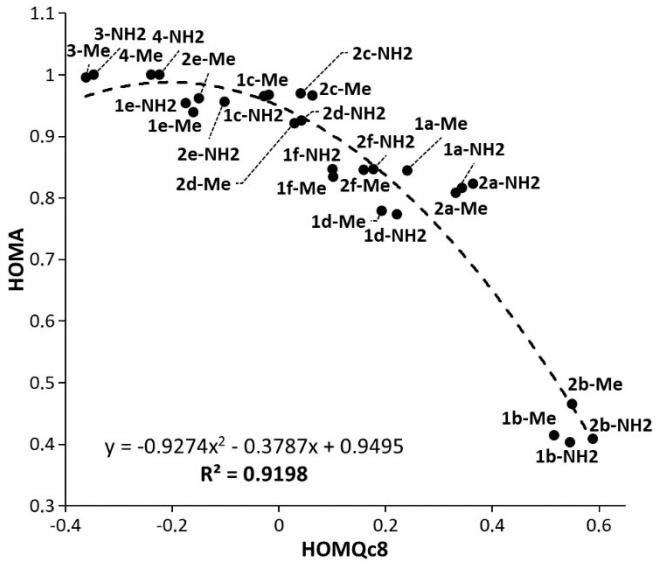

Figure 3. HOMA values plotted against HOMQc8 with a second-order polynomial fit.

can be observed in the NICS(1) versus HOMQc8 representation (Figure 4) for i) cationic (**a**) and triplet neutral (**c**) species showing enhanced magnetic aromatic response, ii) neutral singlet (**b**) and triplet di-anionic (**f**) species together with unligated monoanionic (**1 d**) and singlet dianionic (**1 e**) derivatives, with low magnetic aromatic response, and iii) intermediate behaviour for complexes of the two latter families (**2 d** and **2 e**).

Interestingly, three different groups of compounds with low, medium and high aromaticity are observed when plotting NICS(1) against the *p*-quinodimethane character (Figure 4), HOMQc8 giving rise to better linear response than HOMQc6

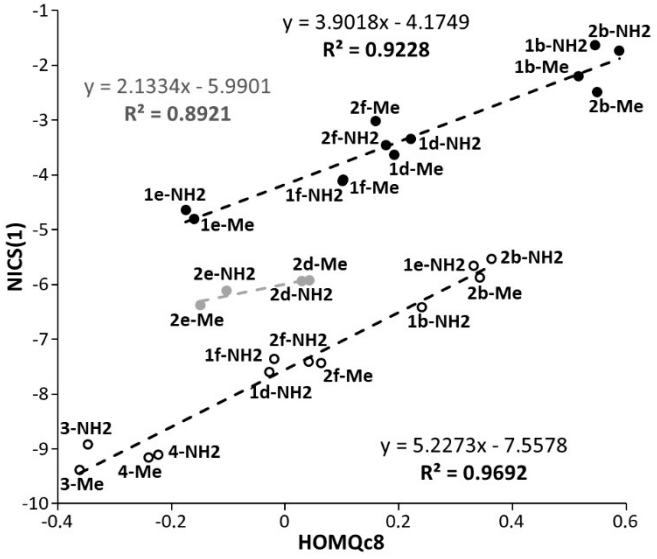

Figure 4. NICS(1) values (ppm) plotted against HOMQc8 with linear fits for the three separated groups of compounds.

(Figure S1) according to the R^2 data. Compounds with the lowest (**b**, **f**, **1 d** and **1 e**) and highest (**a**, **c**) magnetic aromatic response nicely correlate along all the HOMQc8 range with a low (-4.17 ppm) and high (−7.51 ppm) negative intercept. In between a moderate linear correlation is observed for complexes **2 d** and **2 e** with intermediate magnetic aromatic response (intercept −5.99 ppm).

Derivatives with bulky P-substituents

To further understand these low-aromaticity neutral systems, a new set of derivatives bearing bulky alkyl and amino *P*-substituents, with real application in this field, were used (CPh_3, $CH(SiMe_3)_2$, NPh_2),[24] and with all group 6 metals (Scheme 4), being even known as a pPQDM complex in the literature (**2bIII^W**).[11,14]

According to the FMO (frontier molecular orbital) drawings in these compounds **1 b** and **2 b** (see the Supporting Information), HOMOs display the same pattern as in model derivatives with a quinoid-type arrangement of alternating double bonds, including the two exocyclic bonds, and important contribution of the metal fragment in case of metal complexes (Figure 5 for

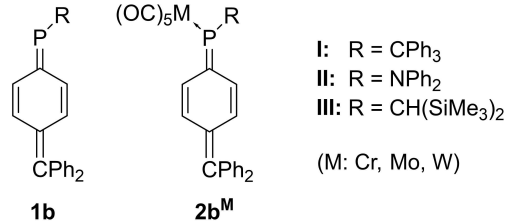

Scheme 4. Structures of the computed compounds **1 b**, **2b^M**.

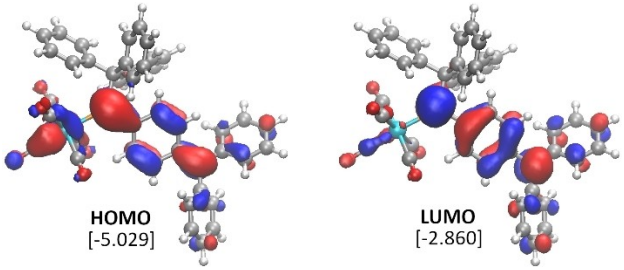

Figure 5. HOMO (left) and LUMO (right) Kohn-Sham isosurfaces (0.03 au) of **2bIW** with their energy given in brackets (in eV).

a case in point for **2bI^{W}**). LUMO contains π* contributions of the exocyclic bonds and comparatively less contribution of the metal fragments, especially in case of the trityl-substituted derivatives **2bI^{M}**.

In order to gain insight into the redox behaviour of these compounds, their chemical hardness (from HOMO and LUMO energies), as well as vertical ionization potentials (IP) and electron affinities (EA) were computed (Table 5). The most noteworthy property is the remarkably low LUMO energies (from −2.916 to −2.518 eV), and hence high EA (from 2.940 to 2.513 eV), as expected for *p*-quinodimethane derivatives that are prone to undergoing reduction in order to acquire an aromatic electronic structure (see structure **2 d** in Scheme 3). As expected, a good correlation is found between these two parameters (linear $R^2 = 0.955$ and second-order polynomial $R^2 = 0.954$ for unligated and complexed derivatives, respectively; see the Supporting Information). The IP is related to the relative tendency to undergo oxidation processes. Higher IP values correspond to lower (more negative) HOMO energies, with a remarkable linear correlation ($R^2 = 0.942$, see the Supporting Information). As expected, the easiest oxidizable molecules are those with *P*-amino substituents (**II**). The chemical hardness (η) of a molecule is connected to its chemical reactivity and has been used,[25] for instance, to discuss the ring strain in saturated three-membered rings[26] or the reactivity in conjugated ring systems.[27] Large HOMO-LUMO gap (chemical hardness) points to unfavourable extraction of electrons from a low-lying HOMO and unfavourable addition of electrons to a high-lying LUMO, therefore corresponding to low reactivity. According to this criterion, *P*-amino-substituted derivatives (**II**) must be expected again to exhibit the highest reactivity, in particular the tungsten complex **2bII^{W}**.

The obtained IP and EA values display a good correlation when plotted against HOMQc8 values (Figure 6 and Figure 7).

Worth is mentioning that all complexes **2b^{M}** give a good (almost linear) second-order polynomial fit of IP against HOMQc8 (Figure 6), with a clear dependency of IP on the P-substituent in the order **2bI^{M}** > **2bIII^{M}** > **2bII^{M}**. No clear metal-dependency is observed, in stark contrast to the observed ease of oxidation for $[M(CO)_5(PR_3)]$[1c] or related phosphorus three- and five-mem-bered heterocyclic complexes.[28] Obviously, the unligated species **1 b** show a different behaviour due to their extra lone pair being involved in the ionization process.

Conclusion

p-Phosphaquinodimethane (pPQDM) derivatives with either simplified model (Me, NH_2) and real (or experimentally plausible) bulky *P*-substituents were computed, in either unligated (**1**) and group 6 κ-*P*-$M(CO)_5$ complexed form (**2**) and with various electronic states from cationic (**a**) to dianionic (**e**,**f**).

Table 5. Computed IP, EA, FMO energies, chemical hardness (eV) and HOMQc6 and HOMQc8 (in parenthesis) for compounds **1bI-III** and **2bI-III** (B3LYP-D3/def2-TZVP(ecp)/COSMO(THF)).

	IP	EA	E_{HOMO}	E_{LUMO}	η	HOMQc6/8
1bI	5.110	2.705	−5.077	−2.750	2.33	0.616 (0.508)
2bI^{Cr}	5.064	2.927	−5.065	−2.916	2.15	0.523 (0.498)
2bI^{Mo}	5.064	2.915	−5.082	−2.852	2.23	0.526 (0.507)
2bI^{W}	5.047	2.940	−5.029	−2.860	2.17	0.516 (0.504)
1bII	4.780	2.562	−4.779	−2.527	2.25	0.592 (0.514)
2bII^{Cr}	4.926	2.783	−4.887	−2.666	2.22	0.555 (0.552)
2bII^{Mo}	4.915	2.808	−4.901	−2.747	2.15	0.540 (0.550)
2bII^{W}	4.917	2.837	−4.873	−2.767	2.11	0.532 (0.549)
1bIII	4.952	2.513	−4.940	−2.518	2.42	0.618 (0.517)
2bIII^{Cr}	4.972	2.665	−4.956	−2.592	2.36	0.584 (0.530)
2bIII^{Mo}	4.966	2.700	−4.996	−2.651	2.35	0.570 (0.528)
2bIII^{W}	4.958	2.728	−4.965	−2.657	2.31	0.560 (0.525)

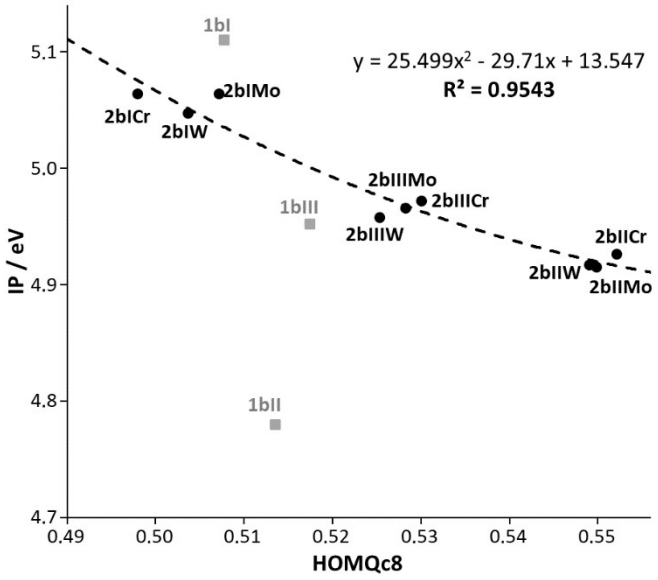

Figure 6. IP values plotted against HOMQc8 with polynomial fit for the complexed derivatives.

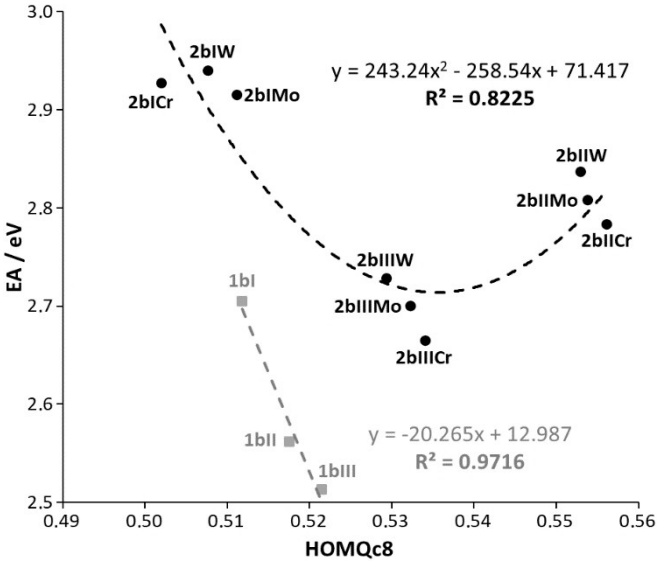

Figure 7. EA values plotted against HOMQc8 with linear/second-order polynomial fits for the two separated groups of compounds.

In model species, P–W and P–N bonds decrease their strength on increasing the electric charge of the system. Singlet neutral species (**b**) display the shortest (highest order) pPQDM exocyclic bonds, whereas the largest (weakest) ones are exhibited by the corresponding triplet states (**c**) and specially singlet dianions (**e**). The spin density is mainly located at P for unligated Me-substituted radical cations (**1 a-Me**), the unpaired electron being pushed to the trityl-derived moiety by either amino-substitution (**1 a-NH_2**) and/or P-complexation (**2 a**). The spin density at the metal fragment increases on increasing the overall negative charge, although almost vanishing for radical anions (**2 d**). Very low aromaticity (high quinoid) character is supported by indices such as HOMA and NICS(1) for neutral singlet derivatives (**b**), whereas high aromaticity for neutral triplets (**c**) and somewhat lower for radical cations (**a**). In between, singlet dianions (**e**) exhibit higher aromaticity than radical anions (**d**) and in both cases their behaviour largely depends on their complexation state, being higher for complexes (**2 e** > **2d**) than for unligated derivatives (**1 e** > **1d**). The latter (**1 d**) have similar low aromaticity than triplet dianions (**f**). However, the most accurate descriptor for the geometric distortion comes from a new HOMQc parameter made up by one geometric (GEO) and an enlargement (EN) contribution. Two versions of this parameter make use of the six endocyclic bonds (HOMQc6) or additionally including the two exocyclic bonds (HOMQc8), the latter requiring previous conversion of C–P bonds into virtual C–C bonds through equivalent Pauling Bond Orders. HOMQc6 is almost equivalent to HOMA, whereas HOMQc8 provides good linear correlation with NICS(1) in three subsets for low- (**b**, **1 d**, **f** and **1 e**), medium- (**2 d**, **2 e**) and high-aromaticity (**a**, **c**) derivatives. This furnishes a clear picture of ligand engagement (non-innocence) in the redox chemistry of the resulting metal complexes and a measure of ring deformation to accommodate electron density changes within pPQDM ligands themselves.

In bulky *P*-substituted systems the highest quinoid character (HOMQc8) is observed for the diphenylamino substituent, whereas the lowest corresponds to the trityl group. The vertical ionization potential almost linearly correlates with HOMQc8 within complexes. The vertical electron affinity shows relatively high values (resulting from low lying LUMOs), metal dependency in the order W > Mo > Cr, as well as well-defined separated tendencies for complexed and unligated derivatives with HOMQc8.

Experimental Section

The quantum chemical calculations were done with ORCA 3.0.3 (model compounds) and ORCA 4.0.2[31] (real compounds). Preoptimized geometries utilizing a pure density functional PBE[32] were fully optimized and computed using the B3LYP[33] functional, together with the def2-TZVP *Ahlrichs* basis sets[35] in combination with the *effective core potential* (ECP)[36] for W (ECP-46) and the efficient RIJCOSX algorithm.[37] Additionally all calculations include the semiempiric DFT-D3[38] dispersion correction and COSMO solvent corrections[39] for THF (permittivity constant $\varepsilon = 7.58$ with diameter $R_{solv} = 3.18$ Å). *Kohn-Sham* orbitals[34] and the VMD software[42] were used for visualization (Figure 5) Numerical frequency calculations were performed to check the correct nature of all computed minima (absence of imaginary frequencies). Also, for magnetic shielding ^{31}P NMR calculations, the *Gauge Including Atomic Orbital method* (GIAO)[40] was used, includes all electrons and scalar relativistic effects via ZORA.[41] Computed NICS shifts were referenced against benzene (NICS(1) = −9.90 ppm) computed at the same level of theory (B3LYP/def2-TZVPPD). Parameters for HOMA (R_{opt}(benzene) = 1.392 Å,, $\alpha = 257.7$), HOMQc6 (R_{opt} = 1.396252 Å, $\alpha = 298.4709$) and HOMQc8 (R_{opt} = 1.346627 Å, α = 133.5929) were computed at the same level of theory (B3LYP-D3/def2-TZVP/COSMO(THF)). In case of HOMQc6/8, R_{opt} and α were fitted to normalize the values to 0 and 1 for *p*-xylene and *p*-quinodimethane, respectively.

Acknowledgements

We acknowledge financial support by the Deutsche Forschungsgemeinschaft (STR 411/46-1). The authors wish to thank the Mulliken Centre (University of Bonn) and Servicio de Cálculo Científico (SCC – University of Murcia) for their technical support and the computational resources used. P.J. is thankful to the Bonn International Graduate School (BIGS Chemistry) for financing a one month stay in Murcia. Also, A.R.P. is indebted to the Erasmus Practicum opportunity (3 month) and the University of Bonn Fellowship Programme (3 month) for financing short stays in Bonn. Open access funding enabled and organized by Projekt DEAL.

Conflict of Interest

The authors declare no conflict of interest.

Keywords: Aromaticity · DFT calculations · geometric distortion · NICS · phosphaquinodimetane

[1] a) W. Kaim, *Inorg. Chem.* **1984**, *23*, 504–505; b) P. Neta, E. Huie, A. B. Ross, *J. Phys. Chem. Ref. Data* **1989**, *17*, 1027–1038; c) N. G. Connelly, W. E. Geiger, *Chem. Rev.* **1996**, *96*, 877–910; d) K. E. Toccara, L. McElwee-White, *Coord. Chem. Rev.* **2000**, 206–207, 469–491.

[2] a) M. Niemeyer, P. P. Power, *Inorg. Chem.* **1997**, *36*, 4688; b) S. T. Haubrich, P. P. Power, *J. Am. Chem. Soc.* **1998**, *120*, 2202; c) M. Niemeyer, P. P. Power, *Angew. Chem. Int. Ed.* **1998**, *37*, 1277; *Angew. Chem.* **1998**, *110*, 1291; d) S. Jockusch, J. Turro, *J. Am. Chem. Soc.* **1998**, *120*, 11773–11777; e) S. Sasaki, K. Sutoh, F. Murakami, M. Yoshifuji, *J. Am. Chem. Soc.* **2002**, *124*, 14830–14831; f) D. Heift, Z. Benkő, H. Grützmacher, *Angew. Chem. Int. Ed.* **2014**, *53*, 6757–6761; *Angew. Chem.* **2014**, *126*, 6875–6879.

[3] a) A. Jouaiti, A. Al Badri, M. Geoffroy, G. Bernadinelli, *J. Organomet. Chem.* **1997**, *529*, 143–149; b) H. Sidorenkova, M. Chentit, S. Chona, M. Geoffroy, Y. Ellinger, *Phys. Chem. Chem. Phys.* **2002**, *4*, 4931–4936; c) C. Dutan, S. Shah, R. C. Smith, S. Chona, T. Berclaz, M. Geoffroy, J. D. Protasiewicz, *Inorg. Chem.* **2003**, *42*, 6241–6251; d) M. Yoshifuji, A. J. Arduengo III, T. A. Konovalova, L. D. Kispert, M. Kikuchi, S. Ito, *Chem. Lett.* **2006**, *35*, 1136–1137; e) O. Back, M. A. Celik, G. Frenking, M. Melaimi, B. Donnadieu, G. Bertrand, *J. Am. Chem. Soc.* **2010**, *132*, 10262–10263; f) M. Lejeune, P. Grosshans, T. Berclaz, H. Sidorenkova, C. Besnard, P. Pattison, M. Geoffroy, *New J. Chem.* **2011**, *35*, 2510–2520; g) X. Pan, X. Wang, Y. Zhao, Y. Sui, X. Wang, *J. Am. Chem. Soc.* **2014**, *136*, 9834–9837; h) F. Hirakawa, H. Ichikawa, S. Ishida, T. Iwamoto, *Organometallics* **2015**, *34*, 2714–2716; i) G. Tan, S. Li, S. Chen, Y. Sui, Y. Zhao, X. Wang, *J. Am. Chem. Soc.* **2016**, *138*, 6735–6738; j) Z. Li, Y. Hou, Y. Li, A. Hinz, J. R. Harmer, C.-Y. Su, G. Bertrand, H. Grützmacher, *Angew. Chem. Int. Ed.* **2018**, *57*, 198–202; *Angew. Chem.* **2018**, *130*, 204–208.

[4] a) T. J. Meyer, *Acc. Chem. Res.* **1978**, *11*, 94–100; b) W. Kaim, *Coord. Chem. Rev.* **1987**, *76*, 187–235; c) H.-J. Grützmacher, *Angew. Chem. Int. Ed.* **2008**, *47*, 1814–1818 Angew. Chem. **2008**, 120, 1838–1842; d) H. Li, M. B. Hall, *J. Am. Chem. Soc.* **2015**, *137*, 12330–12342.

[5] a) A. H. Cowley, R. A. Kemp, J. C. Wilburn, *J. Am. Chem. Soc.* **1982**, *104*, 331–332; b) F. F. Puschmann, J. Harmer, D. Stein, H. Rüegger, B. de Bruin, H. Grützmacher, *Angew. Chem. Int. Ed.* **2010**, *49*, 385–389; *Angew. Chem.* **2010**, *122*, 395–399; c) X. Yang, T. L. Gianetti, J. Harbort, M. D. Wörle, L. Tan, C.-Y. Su, P. Jurt, J. R. Harmer, H. Grützmacher, *Angew. Chem. Int. Ed.* **2016**, *55*, 11999–12002; *Angew. Chem.* **2016**, *128*, 12178–12181.

[6] a) L. A. Berben, *Chem. Eur. J.* **2015**, *21*, 2734–2742; b) A. R. Corcos, O. Villanueva, R. C. Walroth, S. K. Sharma, J. Bacsa, K. M. Lancaster, C. E. MacBeth, J. F. Berry, *J. Am. Chem. Soc.* **2016**, *138*, 1796–1799; c) H. C. Wan, J.-X. Zhang, C. S. Leung, F. K. Sheong, Z. Lin, *Dalton Trans.* **2019**, *48*, 14801–14807; d) J. Abbenseth, D. Delony, M. C. Neben, C. Würtele, B. de Bruin, S. Schneider, *Angew. Chem. Int. Ed.* **2019**, *58*, 6338–6341; *Angew. Chem.* **2019**, *131*, 6404–6407.

[7] a) S. L. Hinchley, C. A. Morrison, D. W. H. Rankin, C. L. B. Macdonald, R. J. Wiacek, A. H. Cowley, M. F. Lappert, G. Gundersen, J. A. C. Clyburne, P. P. Power, *Chem. Commun.* **2000**, 2045–2046; b) J.-P- Bezombes, K. B. Borisenko, P. B. Hitchcock, M. F. Lappert, J. E. Nycz, D. W. H. Rankin, H. E. Robertson, *Dalton Trans.* **2004**, 1980–1988; c) J.-P- Bezombes, P. B. Hitchcock, M. F. Lappert, J. E. Nycz, *Dalton Trans.* **2004**, 499–501.

[8] a) B. Ndiaye, S. Bhat, A. Jouaiti, T. Berclaz, G. Bernardinelli, M. Geoffroy, *J. Phys. Chem. A* **2006**, *110*, 9736–9742; b) T. Berclaz, B. Ndiaye, S. Bhat, A. Jouaiti, M. Geoffroy, *Chem. Phys. Lett.* **2007**, *440*, 224–228; c) H. Sidorenkova, T. Berclaz, B. Ndiaye, A. Jouaiti, M. Geoffroy, *J. Phys. Chem. Solids* **2009**, *70*, 713–718; d) I. Danila, F. Biaso, H. Sidorenkova, M. Geoffroy, M. Fourmigué, E. Levillain, N. Avarvari, *Organometallics* **2009**, *28*, 3691–3699.

[9] a) T. Heurich, V. Nesterov, G. Schnakenburg, Z.-W. Qu, S. Grimme, K. Hazin, D. P. Gates, M. Engeser, R. Streubel, *Angew. Chem. Int. Ed.* **2016**, *55*, 14439–14443; b) T. Heurich, Z.-W. Qu, G. Schnakenburg, Y. Nejaty Jahromy, O. Schiemann, S. Grimme, R. Streubel, *Organometallics* **2017**, *36*, 2877–2883; c) T. Heurich, N. R. Naz, Z.-W. Qu, G. Schnakenburg, R. Streubel, *Organometallics* **2018**, *37*, 3670–3677; d) T. Heurich, Z.-W. Qu, R. Kunzmann, G. Schnakenburg, M. Engeser, S. Nožinović, R. Streubel, *Chem. Eur. J.* **2018**, *24*, 6473–6478.

[10] a) C. Gouverd, M. Brynda, T. Berclaz, M. Geoffroy, *J. Organomet. Chem.* **2006**, *691*, 72–78; b) M. Klein, C. Albrecht, G. Schnakenburg, R. Streubel, *Organometallics* **2013**, *32*, 4938–4943.

[11] a) F. Murakami, S. Sasaki, M. Yoshifuji, *J. Am. Chem. Soc.* **2005**, *127*, 25; b) A. Özbolat-Schön, M. Bode, G. Schnakenburg, A. Anoop, M. van Gastel, F. Neese, R. Streubel, *Angew. Chem. Int. Ed.* **2010**, *49*, 6894–6898.

[12] E. B. Garner III, A. J. Arduengo III, R. Streubel, D. A. Dixon, *Dalton Trans.* **2014**, *43*, 2069.

[13] a) B. F. Yates, W. J. Bouma, L. Radom, *J. Am. Chem. Soc.* **1984**, *106*, 5805; b) B. F. Yates, W. J. Bouma, L. Radom, *Tetrahedron* **1986**, *42*, 6225; c) H. Helten, C. Neumann, A. Espinosa, P. G. Jones, M. Nieger, R. Streubel, *Eur. J. Inorg. Chem.* **2007**, 4669–4678; d) H. Helten, S. Fankel, O. Feier-Iova, M. Nieger, A. Espinosa Ferao, R. Streubel, *Eur. J. Inorg. Chem.* **2009**, 3226–3237; e) X. Chen, L. L. Liu, S. Liu, H. Grützmacher, Z. Li, *Angew. Chem. Int. Ed.* **2020**, *59*, 23830–23835; *Angew. Chem.* **2020**, *132*, 24038–24043.

[14] P. Junker, J. M. Villalba Franco, G. Schnakenburg, V. Nesterov, R. T. Boeré, Z.-W. Qu, R. Streubel, *Dalton Trans.* **2020**, *49*, 13544–13548.

[15] a) I. Mayer, *Chem. Phys. Lett.* **1983**, *97*, 270–274; b) I. Mayer, *Int. J. Quantum Chem.* **1984**, *26*, 151–154; c) I. Mayer, *Theor. Chim. Acta* **1985**, *67*, 315–322; d) I. Mayer, *Modelling of Structure and Properties of Molecules*, John Wiley & Sons, New York, Chichester, Brisbane, Toronto, **1987**; e) A. J. Bridgeman, G. Cavigliasso, L. R. Ireland, J. Rothery, *J. Chem. Soc. Dalton Trans.* **2001**, 2095–2108.

[16] P.-O. Löwdin, *J. Chem. Phys.* **1950**, *18*, 365.

[17] Natural charges were also computed for a small set of model compounds, showing similar tendencies.

[18] J. Poater, X. Fradera, M. Durán, M. Solà, *Chem. Eur. J.* **2003**, *9*, 400–406.

[19] E. Matito, M. Duran, M. Solà, *J. Chem. Phys.* **2005**, *122*, 014109.

[20] P. v. Ragué Schleyer, C. Maerker, A. Dransfeld, H. Jiao, N. J. R. v. Eikema Hommes, *J. Am. Chem. Soc.* **1996**, *118*, 6317.

[21] a) J. Kruszewski, T. M. Krygowski, *Tetrahedron Lett.* **1972**, *13*, 3839–3842; b) T. M. Krygowski, *J. Chem. Inf. Comput. Sci.* **1993**, *33*, 70–78; c) T. M. Krygowski, M. Cyrański, *Tetrahedron.* **1996**, *52*, 1713–1722; d) T. M. Krygowski, M. Cyrański, *Tetrahedron.* **1996**, *52*, 10255–10264; e) T. M. Krygowski, M. Cyrański, *Chem. Rev.* **2001**, *101*, 1385–1420; f) A. Espinosa, A. Frontera, R. García, M. A. Soler, A. Tárraga, *Arkivoc.* **2005**, *ix*, 415–437.

[22] A. Espinosa Ferao, R. García, *Tetrahedron* **2017**, *73*, 952–956.

[23] A. Espinosa Ferao, A. García Alcaraz, R. García López, *New J. Chem.* **2021**, *45*, 4472–4480.

[24] a) A. Özbolat Schön, G. v. Frantzius, J. M. Peréz, M. Nieger, R. Streubel, *Angew. Chem. Int. Ed.* **2007**, *46*, 9327–9330; *Angew. Chem.* **2007**, *119*, 9488–9491; b) V. Nesterov, G. Schnakenburg, A. Espinosa, R. Streubel, *Inorg. Chem.* **2012**, *51*, 12343–12349; c) P. Junker, Z.-W. Qu, T. Kalisch, G. Schnakenburg, A. Espinosa Ferao, R. Streubel, *Dalton Trans.* **2021**, *50*, 739.

[25] a) R. G. Pearson, *Coord. Chem. Rev.* **1990**, *100*, 403–425; b) Z. Zhou, R. G. Parr, J. F. Garst, *Tetrahedron Lett.* **1988**, *29*, 4843–4846; c) Z. Zhou, R. G. Parr, *J. Am. Chem. Soc.* **1989**, *111*, 7371–7379; d) R. G. Parr, Z. Zhou, *Acc. Chem. Res.* **1993**, *26*, 256–258; e) G. Makov, *J. Phys. Chem.* **1995**, *99*, 9337–9339; f) Y.-Z. Huang, S.-Y. Yang, X.-Y. Li, *J. Organomet. Chem.* **2004**, *689*, 1050–1056.

[26] A. Rey Planells, A. Espinosa Ferao, *Inorg. Chem.* **2020**, *59*, 11503–11513.
[27] Z. Zhou, R. G. Parr, *J. Am. Chem. Soc.* **1990**, *112*, 5720–5724.
[28] H. Helten, S. Fankel, O. Feier-Iova, M. Nieger, A. Espinosa, R. Streubel, *Eur. J. Inorg. Chem.* **2009**, 3226–3237.
[29] a) W. P. Jencks, J. Carriuolo, *J. Am. Chem. Soc.* **1960**, *82*, 1778–86; b) W. P. Jencks, J. Carriuolo, *J. Am. Chem. Soc.* **1960**, *82*, 75–81; c) J. O. Edwards, R. G. Pearson, *J. Am. Chem. Soc.* **1962**, **84**, 16–24; d) Y. Ren, H. Yamataka, *J. Org. Chem.* **2007**, *72*, 5660–5667.
[30] P. P. Power, *Chem. Rev.* **2003**, *103*, 789–809.
[31] F. Neese, *Wiley Interdiscip. Rev.: Comput. Mol. Sci.* **2012**, 2, 73–78.
[32] J. P. Perdew, K. Burke, M. Ernzerhof, *Phys. Rev. Lett.* **1996**, *77*, 3865.
[33] a) P. J. Stephens, F. J. Devlin, C. F. Chabalowski, M. J. Frisch, *J. Phys. Chem.* **1994**, *98*, 11623; b) A. D. Becke, *Phys. Rev. A* **1988**, *38*, 3098; c) C. Lee, W. Yang, R. G. Parr, *Phys. Rev. A* **1988**, *37*, 785.
[34] a) P. Hohenberg, W. Kohn, *Phys. Rev.* **1964**, *136*, 864–871; b) W. Kohn, L. J. Sham, *Phys. Rev.* **1965**, *140*, A1133–A1138.
[35] a) F. Weigend, R. Ahlrichs, *Phys. Chem. Chem. Phys.* **2005**, *7*, 3297–3305; b) F. Weigend, M. Häser, H. Patzelt, R. Ahlrichs, *Chem. Phys. Lett.* **1998**, *294*, 143–152; c) F. Weigend, R. Ahlrichs, *Phys. Chem. Chem. Phys.* **2005**, *7*, 3297–3305; d) F. Weigend, F. Furche, R. Ahlrichs, *J. Chem. Phys.* **2003**, *119*, 12753–12762.
[36] a) B. Metz, H. Stoll, M. Dolg, *J. Chem. Phys.* **2000**, *113*, 2563–2569; b) K. A. Peterson, D. Figgen, E. Goll, H. Stoll, M. Dolg, *J. Chem. Phys.* **2003**, *119*, 11113–11123; c) A. Schaefer, H. Horn, R. Ahlrichs, *J. Chem. Phys.* **1992**, *97*, 2571.
[37] C. Hättig, F. Weigend, *J. Chem. Phys.* **2000**, *113*, 5154–5161.
[38] a) S. Grimme, J. Antony, S. Ehrlich, H. Krieg, *J. Chem. Phys.* **2010**, *132*, 154104; b) S. Grimme, S. Ehrlich, L. Goerigk, *J. Comput. Chem.* **2011**, *32*, 1456–1465.
[39] a) A. Klamt, G. Schüürmann, *J. Chem. Soc. Perkin Trans. 2* **1993**, 799–805; b) F. Eckert, A. Klamt, *AIChE J.* **2002**, *48*, 369–385; c) S. Sinnecker, A. Rajendran, A. Klamt, M. Diedenhofen, F. Neese, *J. Phys. Chem. A* **2006**, *110*, 2235–2245.
[40] T. Ziegler, G. Schreckenbach, *J. Phys. Chem.* **1995**, *99*, 606–611.
[41] a) E. Van Lenthe, E. J. Baerends, J. G. Snijders, *J. Chem. Phys.* **1993**, *99*, 4597; b) C. van Wuellen, *J. Chem. Phys.* **1998**, *109*, 392.
[42] W. Humphrey, A. Dalke, K. Schulten, *J. Molec. Graphics* **1996**, *14*, 33–38.

Manuscript received: February 2, 2021
Accepted manuscript online: April 3, 2021
Version of record online: May 21, 2021

